Sensors and Materials, Vol. 36, No. 7 (2024) 2943–2953
MYU Tokyo

S & M 3711

Temperature Optical Sensor Made of Recycled Waste Materials and Implementation of Machine Learning Method to Expand Its Measurement Range

Sergio Ivan Ramirez-Zavala, Everardo Vargas-Rodriguez, Ana Dinora Guzman-Chavez,* and Oscar Manuel Salazar-Martinez

Universidad de Guanajuato,
División de Ingenierías, Departamento de Estudios Multidisciplinarios, Yuriria 38940, México

(Received February 21, 2024; accepted June 20, 2024)

Keywords: tunable optical interferometer, temperature sensor, recycled waste materials, machine learning, kernel ridge regression

The efficient use of resources can contribute to the eradication of poverty and the reduction of environmental impact. Therefore, the use of recycled waste materials is desirable since it helps in the reduction of pollution. Some devices, such as interferometric optical sensors, can be implemented with this type of materials. In addition, optical sensors play an important role in the Internet of Things since they can be used to implement networks that simultaneously monitor several physical parameters. A problem that limits the measurement range of interferometric optical sensors is the 2π ambiguity. In this work, it is presented that the nominal measurement range of this type of sensor can be increased considerably by applying machine learning algorithms. In this sense, the kernel ridge regression (KRR) method is applied to the signals of a temperature sensor that is based on a tunable optical two-layer interferometer. Here, it is shown that this interferometric sensor can be fabricated with recycled waste materials (a polished stainless-steel plate, a single-mode fiber, a syringe needle, and epoxy clay), and the fabrication process is described. Furthermore, it is demonstrated that when KRR is used, the measurement range is increased at least two and a half times compared with that reached with traditional methods, and the temperature can be estimated with a root mean square error of 1.97×10^{-5} °C.

1. Introduction

The green economy is a model that prioritizes the practice of sustainable development in all sectors for human well-being.[1,2] For example, in the industrial sector, the efficient use of resources and the reduction of the carbon footprint are essential, which is partly achieved through the recycling of metals. In the education sector, educators from countries that allocate few economic resources to education will be able to divulge scientific knowledge with the help of instruments or devices that can be made with waste materials. These actions, carried out in poor countries, can simultaneously contribute to the eradication of poverty, which is one of the

*Corresponding author: e-mail: ad.guzman@ugto.mx
https://doi.org/10.18494/SAM5026

ISSN 0914-4935

objectives of the green economy and the education of the people. In this sense, the green economy has encouraged researchers to devote their efforts to finding alternatives that impact the care of the environment and the economic development of an organization.[3–6] Some of these alternatives are solutions based on the 3R scheme—reducing, reusing, and recycling—which is one of the precepts of the green economy model. For example, Islas-Islas *et al.* proposed a simultaneous polarization-based phase-shifting interferometric system made with recycled optical components obtained from electronic waste.[3] Prado *et. al* proposed the recycling of polymethyl methacrylate plates used in LCD monitors to produce polymer optical fibers without cladding for sensing systems.[6] Those recycled fibers were used to implement a refractive index sensor, and the authors reported better results than those obtained with a commercial optical fiber.

Optical sensors based on interferometric systems are interesting measurement devices as these can be used in different fields of applications. Some of the advantages of this type of sensor are their high sensitivity, immunity to electromagnetic radiation, small size, and low cost. Furthermore, the physical parameters that can be measured with these optical sensors include temperature, strain, pressure, and refractive index.[7–15] There exist different configurations to implement interferometric optical sensors, and some of the most popular are those based on Fabry-Perot configurations.[8–13] Some sensors based on interferometers are fabricated mainly with SiO_2 optical fibers. This material is practically insensitive to temperature, which can be important in sensing applications since undesirable effects induced by changes in its temperature can be minimized. Generally, these interferometers are tuned by changing their cavity length by mechanical means.[8,16] The disadvantage of this type of tuning mechanism is that, in many cases, the spectral response can be shifted by less than one free spectral range (FSR). For example, Duan *et al.* proposed a microbubble-based fiber-optic Fabry–Perot interferometer for strain measurement. Here, the spectrum was shifted less than one FSR and the strain and thermal sensitivities were ~4 pm/με and ~0.9 pm/°C, respectively.[8] In this sense, the authors did not propose the interferometer as temperature sensor because of its low thermal sensitivity. Other interferometers are based on layers of thermosensitive materials in which at least one FSR can be tuned by means of a temperature variation.[11–13] For example, Ma *et al.* implemented a dual-polymer fiber Fizeau interferometer for the simultaneous measurement of relative humidity and temperature.[7] By taking advantage of the thermal properties of the polymer, the output spectrum was shifted when a temperature change was applied. Also in that work, the temperature value was obtained by tracking one peak of the output spectrum. Here, it is important to mention that although the interferometric optical sensors are sensitive over a wide temperature range, the measurement range is limited to one FSR owing to the 2π ambiguity, the main limitation of traditional measurement methods. This limitation can be overcome by implementing artificial intelligence algorithms.[12,17,18] These algorithms are based on multiple features of the cases used for training and testing. Furthermore, as most of the output signals of optical interferometers present changes in both wavelength and amplitude, it is possible to extract multiple features. For example, Martinez-Manuel *et al.* used machine learning in refractive index measurements.[17] Here, the measurement device was a self-referenced fiber refractometer. In addition, Guzman-Chavez and Vargas-Rodriguez proposed the use of a multiple regression model for the

simultaneous measurement of refractive index and temperature using an interferometric optical system.[18] In that work, a set of 27 explanatory variables were used with their corresponding values extracted from the output reflective spectrum.

In this work, the fabrication and characterization of an optical sensor based on a tunable two-layer interferometer (T-LI) made with recycled waste materials are proposed. Here, it is important to mention that the efficiency of this physical sensor was not sacrificed by using this type of material. Moreover, the materials used for implementing the interferometer are a polished stainless-steel plate, a needle from a syringe, epoxy clay, cyanoacrylate, and a piece of standard single-mode optical fiber. Here, by taking advantage of the thermal expander (sleeve made of epoxy clay) properties, the fringe pattern is shifted by one free spectral range (22 nm) by applying a temperature change of 7 °C. The experimental results are in agreement with the theoretical results, which were obtained by applying the reflected principal rays summation theory. Finally, it is shown that this tunable interferometric filter can be used to implement a temperature sensor with a broad measurement range when their spectral features are analyzed with kernel ridge regression (KRR). Here, three features of the reflective spectra were used as inputs of the exponential kernel to determine the temperature with high accuracy.

2. Fabrication and Operation of Tunable T-LI

The tunable T-LI was fabricated with recycled waste materials such as a polished stainless-steel plate, a syringe needle, and a piece of standard single-mode optical fiber. The steps for manufacturing the filter (Fig. 1) are as below.

1. Clean with acetone one surface of a polished stainless-steel plate. Also, cut and clean a piece of unused syringe needle (~1.2 cm).
2 Place the piece of needle vertically on the cleaned surface of the steel plate and then deposit a sleeve of thermosensitive epoxy clay around the piece of needle and over the cleaned plate. Here, the epoxy clay is used to hold the needle segment perpendicularly over the plate.
3. Remove the fiber coating (~3 cm) from the end of a piece of standard optical fiber (~50 cm), preferably without removing the outer jacket. In case it is removed, thicken the fiber with a resin to match the internal diameter of the needle. Afterwards, introduce the fiber, cleaved with a face angle of 0°, into the needle channel with a 3-axis positioner. This is used to control the distance between the fiber end and the plate surface.

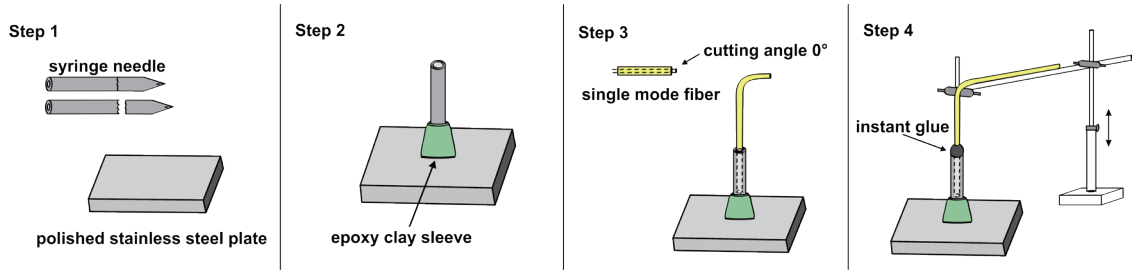

Fig. 1. (Color online) Fabrication steps of the tunable T-LI interferometer using recycled waste materials.

4. To create the first layer, place the fiber a certain distance from the plate, then introduce cyanoacrylate through the syringe and wait for it to dry. For the second air layer, separate the fiber from the cyanoacrylate layer by a certain distance and glue the optical fiber to the end of the piece of needle. Ultimately, the other end of the optical fiber will be used to launch light to the device, rendering it a pigtailed tunable optical T-LI.

2.1 Principle of operation of two-layer interferometer

The two-layer interferometer is formed of two stacked layers of infrared transparent materials. Its relative reflectance spectrum (R) is governed by the superposition of multiple reflections between their interfaces (Fig. 2). The reflection intensities that form the fringe spectrum depend on the refractive indexes of the materials that form these interfaces. The separation between fringes is governed mainly by the refractive indexes and the thicknesses of the layers. Here, when the thickness of one of the layers depends on an external expander made of a thermosensitive material [Fig. 3(a)], the fringe spectrum can be tuned by adjusting the temperature. The mathematical model of a tunable T-LI with a thermal expander can be expressed as

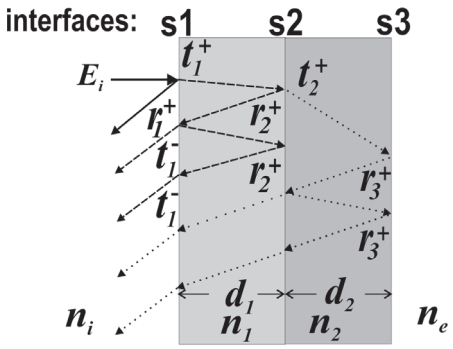

Fig. 2. Reflections between the interfaces that delimit the layers of the T-LI.

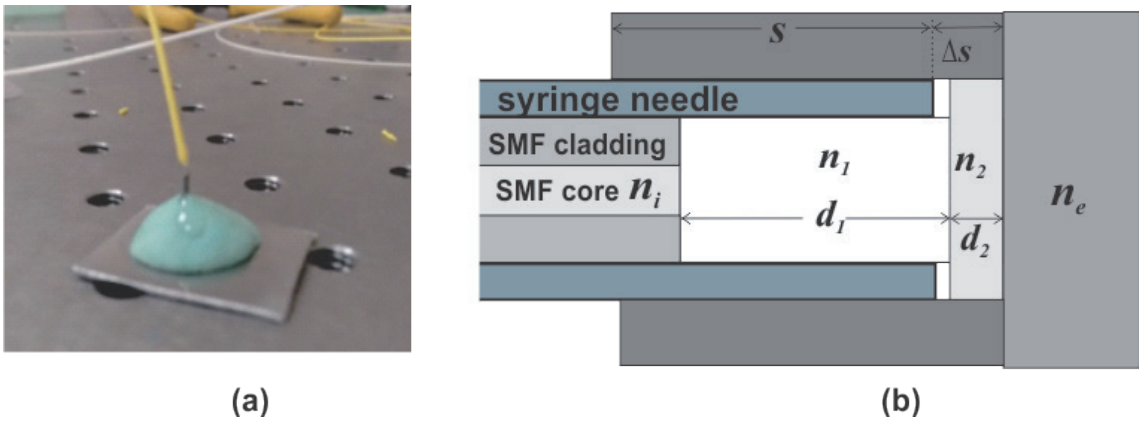

Fig. 3. (Color online) (a) Photograph of the T-LI interferometer fabricated using recycled waste materials and (b) physical model of the tunable T-LI.

$$R = \left|\frac{E_o}{E_i}\right|^2 = \left| \begin{array}{l} r_1^+ + \left(t_1^+\right)^2 \sum_{m=1}^{q} \left(A_1 r_2^+\right)^m \left(-r_1^+\right)^{m-1} \exp\left(i4\pi n_1 d_1(T)/\lambda\right) + \\ \left(t_1^+\right)^2 \left(t_2^+\right)^2 A_1 \sum_{m=1}^{q} \left(A_2 r_3^+\right)^m \left(-r_3^+\right)^{m-1} \exp\left(i4\pi\left(n_1 d_1(T) + m n_2 d_2(T)\right)/\lambda\right) \end{array} \right|^2, \quad (1)$$

where λ is the wavelength, A_1 and A_2 are the factors associated with optical losses, and d_a and d_c are the thicknesses of layers at temperature T. Additionally, $d_a(T) = d_1 + \Delta s$, where $\Delta s = s\gamma_s (T - T_o)$, $d_c(T) = d_1 (1 + \gamma_2(T - T_o))$, $r_1^+ = (n_i - n_1)(n_i + n_1)^{-1}$, $r_2^+ = (n_1 - n_2)(n_1 + n_2)^{-1}$, $r_3^+ = (n_2 - n_e)(n_2 + n_e)^{-1}$, $t_1^+ = (2n_i)(n_i + n_1)^{-1}$, and $t_2^+ = (2n_1)(n_1 + n_2)^{-1}$, where n_i, n_1, n_2, and n_e are refractive indexes, d_1, d_2, and s are the thicknesses of the layers and the length of the thermo-expander, respectively, at T_o = 22.5 °C, and γ_s and γ_2 are thermal-expansion coefficients. Finally, it is important to mention that the reflectance spectrum can be modeled with the first q reflected rays when the reflectance of the interfaces is low.

2.2 Mathematical model of KRR

In the KRR approach, the value of the output variable, $\hat{y}$, can be estimated as a function of a set of features, $\boldsymbol{x}_m \in \boldsymbol{X}$, and of the outcome values associated with $\boldsymbol{x}_m$, $\boldsymbol{y}_n \in \boldsymbol{Y}$, with the following expressions:

$$\hat{y}\left(\boldsymbol{x}_m\right) = \boldsymbol{\beta}^T \boldsymbol{k}\left(\boldsymbol{X}, \boldsymbol{x}_m\right) \quad (2)$$

$$\boldsymbol{\beta} = \left(\boldsymbol{K} + \varepsilon \boldsymbol{I}\right)^{-1} \boldsymbol{Y}, \quad (3)$$

where $\boldsymbol{x}_m = [x_1\ x_2\ x_3\ \ldots\ x_f]^T$ is a column vector that contains the features of the m-th case; f the number of features; $\boldsymbol{X} = [\boldsymbol{x}_1\ \boldsymbol{x}_2\ \boldsymbol{x}_3\ \ldots\ \boldsymbol{x}_N]^T$ an $f \times N$ matrix; N the total number of cases; $\boldsymbol{Y} = [y_1\ y_2\ y_3\ \ldots\ y_N]^T$ a column vector; $k(\boldsymbol{x}_i, \boldsymbol{x}_j)$ a kernel of which one of the most used is the exponential kernel expressed as $k(\boldsymbol{x}_i, \boldsymbol{x}_j) = \exp(-\|\boldsymbol{x}_i - \boldsymbol{x}_j\|/\sigma^2)$, where σ is a real coefficient; $\boldsymbol{k}(\boldsymbol{X}, \boldsymbol{x}_m) = [k(\boldsymbol{x}_1, \boldsymbol{x}_m)\ k(\boldsymbol{x}_2, \boldsymbol{x}_m)\ k(\boldsymbol{x}_3, \boldsymbol{x}_m)\ \ldots\ k(\boldsymbol{x}_N, \boldsymbol{x}_m)]^T$ a column vector; $\boldsymbol{K}_{ij} = k(\boldsymbol{x}_i, \boldsymbol{x}_j)$ the $N \times N$ matrix kernel; $\boldsymbol{\beta}$ an $1 \times N$ row vector that contains the regression coefficients; $\varepsilon > 0$ a real regularization parameter; and $\boldsymbol{I}$ an $N \times N$ identity matrix.

3. Results

3.1 Fabrication of the tunable T-LI

The tunable optical T-LI was fabricated by the steps described above. The materials used were a 3-cm-long piece of a syringe needle with external and internal diameters of 0.81 and 0.51 mm, respectively, a single-mode optical fiber, commercial liquid cyanoacrylate glue, commercial epoxy clay, and a stainless-steel plate (grade 304, thickness 1.55 mm, and matte surface finish)

with a surface of area ~4 cm^2. Here, it is important to mention that the needle was taken from a damaged sterile syringe that was discarded and that it had not been in contact with biological material. Additionally, to have a reflective surface, the plate was polished until a mirror effect was obtained. The photograph of the fabricated multilayer interferometer is shown in Fig. 3(a), in which the materials used to fabricate the interferometer can be observed. Here, it is important to mention that in step 3, we did not remove the outer jacket of the optical fiber, but it was partially worn away.

After fabrication, the tunable T-LI was characterized theoretically and experimentally. For the first characterization, the mathematical model was obtained using the physical model shown in Fig. 3(b). The following numerical values were used to obtain the simulated results: refractive indexes n_i = 1.45, n_1 = 1.0, n_2 = 1.45, and n_e = 2.8 of the fiber core, air, cyanoacrylate, and stainless steel, respectively, d_1 = 52.08 μm, d_2 = 1.78 μm, s = 3800 μm, γ_s = 26.5 μm/(m K), γ_2 = 198 μm/(m K), $1 \leq T \leq 70$ °C, and λ = 1.5 μm. For simulations, only the three main (q = 3) reflected rays were considered because of the low reflectance at the interfaces. The A_1 and A_2 constants of Eq. (1) can be calculated by minimizing the cost function.[11] In this way, the obtained optimal values for our interferometer were A_1 = 0.43 and A_2 = 0.98. For the experimental characterization, the experimental setup shown in Fig. 4 was used, and the temperature was varied in 34 steps covering a measurement range from 12 to 28.5 °C.

3.2 Implementation of the temperature sensor

The experimental setup used to implement the temperature sensing arrangement is shown in Fig. 4. Here, a pigtailed diode laser emitting at ~980 nm was spliced to the pump port of a wavelength division multiplexer (WDM). The light of the diode was used to pump an erbium-doped fiber (EDF) that was spliced to the common port of the WDM. The other end of the EDF was spliced to port 1 of the optical circulator to allow the generated luminescence to travel to port 2 of the circulator. This port was spliced to the pigtailed tunable T-LI. Its temperature was stabilized by driving a thermoelectric cooler (TEC). Finally, the reflected signal of the interferometer was collected at port 3 with an optical spectrum analyzer (OSA).

The simulated and measured relative reflected intensity distribution spectra of the fabricated tunable T-LI at three different temperatures are shown in Fig. 5. The FSR is ~22 nm for both types of spectra, which indicates that these have the same periodicity. Regarding the amplitude of the fringes, in Figs. 5(a)–5(c), it is observed that it is not constant; the explanation is that in the last manufacturing step, a thin cyanoacrylate layer was deposited on the stainless plate. This

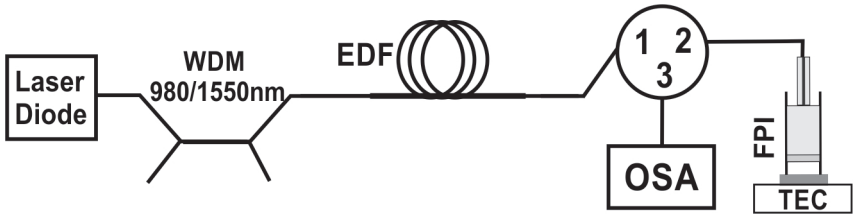

Fig. 4. Experimental setup to characterize the tunable T-LI.

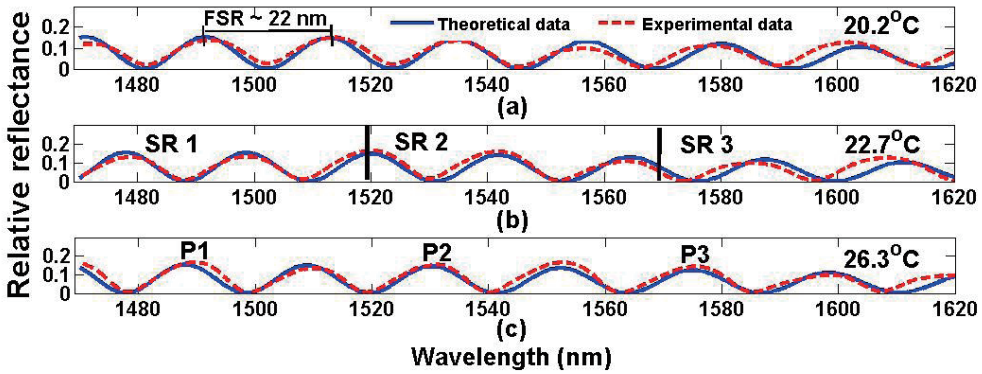

Fig. 5. (Color online) Theoretical and experimental interference spectra at different temperatures of (a) 20.2, (b) 22.7, and (c) 26.3 °C.

allowed the generation of a second spectrum with a longer FSR than that obtained with the air cavity. The resulting spectrum is given as the superposition of two spectra for which the amplitude of the fringes of the spectrum generated by the air cavity is modulated by the spectrum generated by the cyanoacrylate layer.

3.3 Estimation of temperature using KRR

One of the traditional methods of determining the value of the measurand variable is based on the wavelength tracking of one of the peaks of the spectrum. This method is limited by the 2π ambiguity, which consequently limits the measurement range to one FSR. In Fig. 6, the traces of the wavelengths of different fringe peaks are plotted as a function of temperature. These fringes are labeled in Fig. 5(c) as P1, P2, and P3. The red asterisks represent experimental results and the blue dashed lines show the simulated results. It is observed that for all fringes, the linear tuning behavior is repeated periodically when fringes are shifted one FSR. Here, the advantage is that this shifting is completed by applying a relatively small temperature change of 7 °C, because of the high thermal expansion coefficient of the epoxy clay and its length. The disadvantage is that the nominal measurement range width is only of 22 nm, since the peaks of the fringes (the interference spectrum) appear to return to the original position after they have been shifted one FSR. In this sense, to expand the measurement range, the mathematical model of the KRR method was applied.

First, to verify that the KRR method can be used to estimate the sensor temperature values over a larger measurement range, simulated data were used to obtain a synthetic database. Data were obtained from $N = 301$ simulated spectra considering different temperatures within the range from 10 to 70 °C with steps of 0.2 °C. Each spectrum was represented by two vectors, the vector $L_{1500\times1}$ with 1500 wavelength values from 1470 to 1620 and the vector $M_{1500\times1}$ with the amplitudes corresponding to each wavelength. For the extraction of features, each spectrum was divided in three equal spectral regions (SR 1, SR 2, and SR 3), as shown in Fig. 5(b). Here, each spectral region was represented by L_f and M_f vectors with 500 elements. The value of the f-th feature was obtained using $x_f = L^T_f M_f$, where $f = 1, 2, 3$. In this sense, the vector $\boldsymbol{X}$ data matrix

had 3 rows and 301 columns, and the vector $\boldsymbol{Y}$ had 301 temperature values. Subsequently, Eqs. (2) and (3) were used to obtain the estimated values, $\hat{y}(\boldsymbol{x}_m)$, and the root mean square error (*RMSE*), $RMSE = \sqrt{\sum_{m=1}^{N}((\boldsymbol{x}_m) - y_m)/N}$, was calculated to compare the real and estimated temperature values. Here, the σ value was set to 2, and to find the optimal ε value, this was varied 20 times using the equation $\varepsilon_{i+1} = \varepsilon_i/2$ with $\varepsilon_{i=1} = 1$. In Fig. 7(a), the evolution of the *RMSE* value as a function of ε is shown. Here, the optimal ε value was selected as 6.105×10^{-5}, for which $RMSE = 1.3 \times 10^{-3}$ °C. The estimated temperature values obtained with the optimal value were compared with the real temperature values, as shown in Fig. 7(b). It is observed that the two sets of values present a good fit with each other.

The method was then applied to experimental data obtained from $N = 34$ reflected spectra recorded with the OSA with the tunable T-LI at different temperatures. Each spectrum was

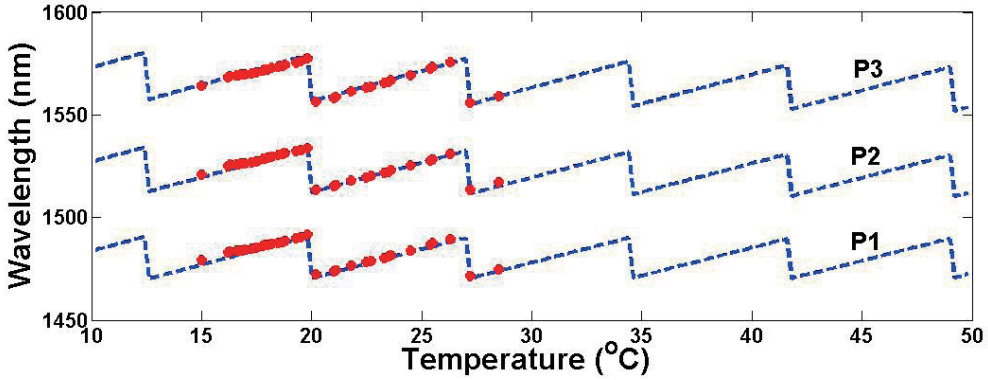

Fig. 6. (Color online) Peak wavelength as a function of temperature for different fringes.

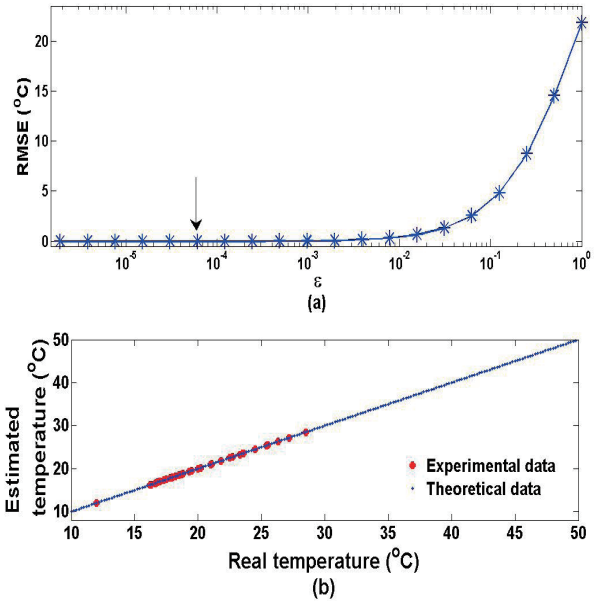

Fig. 7. (Color online) (a) Evolution of the *RMSE* value as a function of the λ value and (b) the real and estimated temperature values obtained with the KRR

divided in three regions, each of which was represented with two vectors, L_f and M_f. In this sense, the data matrix $\boldsymbol{X}$ had 3 rows and 34 columns and the vector $\boldsymbol{Y}$ had 34 measured temperature values. The σ and ε values were the same as those used with the simulated data and $RMSE = 1.97 \times 10^{-5}$ °C was attained. In Fig. 7(b), it can also be observed that the estimated and experimental data have a good fit. Finally, it is important to mention that with the KRR method, it was possible to estimate temperature values within a measurement range at least two and half times greater than that obtained when only one FSR is tuned.

4. Conclusions

In this work, an optical sensor based on a tunable optical interferometer fabricated using recycled materials was presented. It was shown that by using easily accessible recycled waste materials, an efficient tunable T-LI can be fabricated simply and inexpensively. It was also demonstrated that by taking advantage of the thermo-expansion properties of commercial epoxy clay, an optical temperature sensor can be fabricated. Moreover, the fabricated interferometer can be tuned by one FSR = 22 nm with a temperature change of 7 °C, and its experimental performance was supported by the simulation results. Furthermore, it was demonstrated that by using KRR, it is possible to obtain a measurement range greater than that reached when the interferometer is tuned by one FSR, which means that it is possible to overcome the 2π ambiguity of a sensor based on an interferometric filter. Furthermore, this research contributes to the practice of sustainable development and the improvement of sensor properties. Finally, it is important to highlight that the use of machine learning algorithms in optical sensors contributes to improving the monitoring of systems that implement current technologies such as Internet of Things.

References

1 E. Loiseau, L. Saikku, R. Antikainen, N. Droste, B. Hansjürgens, K. Pitkäne, P. Leskinen, P. Kuikman, and M. Thomsen: J. Clean. Prod. **139** (2016) 361. https://doi.org/10.1016/j.jclepro.2016.08.024
2 E. B. Barbier and A. Markandya: A New Blueprint for a Green Economy, Earthscan from Routledge (Routledge, New York, 2013).
3 J. M. Islas-Islas, G. Reséndiz-López, J. G. Ortega-Mendoza, L. García-Lechuga, A. Quiroz, D. I. Serrano Garcia, B. Canales-Pacheco, and N. I. Toto-Arellano: Photonics **9** (2022) 1. https://doi.org/10.3390/photonics9030125
4 J. Islas-Islas, V. H. Flores-Muñoz, D. I. Serrano-García, J. Ortega-Mendoza, M. Durán-Sánchez, A. Guzmán-Barraza, and N.I. Toto-Arellano: Opt. Laser Technol. **123** (2020) 105915. https://doi.org/10.1016/j.optlastec.2019.105915
5 L. Macedo, M. R. W. Pires Junior, A. Frizera, M. J. Pontes, and A. Leal-Junior: Opt. Fiber Technol. **72** (2022) 103001. https://doi.org/10.1016/j.yofte.2022.103001
6 A. R. Prado, A. G. Leal-Junior, C. Marques, S. Leite, G. L. De Sena, L. C. Machado, A. Frizera, M. R. N. Ribeir, and M. J. Pontes: Opt. Express **25** (2017) 30051. https://doi.org/10.1364/OE.25.030051
7 C.-T. Ma, Y.-W. Chang, Y.-J. Yang, and C.-L. Lee: Sensors **17** (2017) 1. https://doi.org/10.3390/s17112659
8 D.-W. Duan, Y.-j. Rao, Y.-S. Hou, and T. Zhu: Appl. Opt. **51** (2012) 1033. https://doi.org/10.1364/AO.51.001033
9 X. Zhang, X. Zhou, S. Wang, P. Tao, F. Ma, Q. Yu, and W. Peng: Sens. Actuators, A **335** (2022) 113375. https://doi.org/10.1016/j.sna.2022.113375
10 E. Vargas-Rodriguez, A. D. Guzman-Chavez, M. Cano-Contreras, E. Gallergo-Arellano, D. Jauregui-Vazquez, J. C. Hernández-García, J. M. Estudillo-Ayala, and R. Rojas-Laguna: Sensors **15** (2015) 26128. https://doi.org/10.3390/s151026128

11 J. Zhang, X. Dong, P. Xu, D. Lv, J. Yang, and Y. Qin: J. Lightwave Technol. **40** (2022) 3010. https://doi.org/10.1109/JLT.2021.3137239
12 A.D. Guzman-Chavez, E. Vargas-Rodriguez, B. L. Vargas-Rodriguez, and M. A. Garcia-Ramirez: IEEE Photonics Technol. Lett. **14** (2022) 915. https://doi.org/10.1109/LPT.2022.3193641
13 M. Jedrzejewska-Szczerska, P. Wierzba, P. Wierzba, A. Abou Chaaya, M. Bechelany, P. Miele, R. Viter, A. Mazikowski, K. Karpienko, and M. Wróbel: Sens. Actuators, A **221** (2015) 88. https://doi.org/10.1016/j.sna.2014.11.001
14 T. Liu, J. Wang, Y. Liao, L. Yang, and S. Wang: Opt. Express **27** (2019) 23905. https://doi.org/10.1364/OE.27.023905
15 C. Zhu and J. Huang: Opt. Lett. **46** (2021) 2180. https://doi.org/10.1364/OL.420618
16 G. Wang, X. Liu, Z. Gui, Y. An, J. Gu, M. Zhang, L. Yan, G. Wang, and Z. Wang: Sensors **17** (2017) 1. https://doi.org/10.3390/s17061192
17 R. Martínez-Manuel, L. M. Valentín-Coronado, J. Esquivel-Hernandez, K. Jean-Jacques Monga, and S. LaRochelle: IEEE Sens. J. **22** (2022) 14134. https://doi.org/10.1109/JSEN.2022.3183475
18 A. D. Guzman-Chavez and E. Vargas-Rodriguez: J. Sens. **2023** (2023) 1. https://doi.org/10.1155/2023/2820062

About the Authors

Sergio Ivan Ramirez-Zavala received his BS degree in communications and electronics from the University of Guanajuato in 2021 and is now pursuing an MS degree in applied electronics at the same university. His current research interests include optical sensors and optoelectronic systems. He is a CONAHCyT scholarship recipient. (sergioivanrz@gmail.com)

Everardo Vargas-Rodriguez completed his M.Sc. degree in instrumentation at the University of Guanajuato, Mexico. Later, he received his Ph.D. degree in optoelectronics from the University of Southampton in 2007. He joined the University of Guanajuato in Mexico in 2007 as a professor. He served as Director of the Department for Multidisciplinary Studies from 2008 to 2016. His research interests include optoelectronics sensors, interferometry, use of machine learning and artificial intelligence on sensor data, and fiber lasers. (evr@ugto.mx)

Ana Dinora Guzman-Chavez received her M.S. and Ph.D. degrees from the Research Center of Optics, Mexico, in 2007 and 2010, respectively. In 2011, she did a postdoctoral study at the University of Valencia, Spain. Since 2012, she has been a professor at Guanajuato University. Her research interests include optical sensors, interferometry, use of machine learning and artificial intelligence on sensor data, and fiber lasers. (ad.guzman@ugto.mx)

Oscar Salazar-Martinez received his BS degree in communications and electronics from the University of Guanajuato in 2021 and is now pursuing an MS degree in applied electronics at the same university. His current research interests include optical sensors and optoelectronic systems. He is a CONAHCyT scholarship recipient. (om.salazarmartinez@ugto.mx)